Intensity and Phase Modulators at 1.55 μm in GaAs/AlGaAs Layers Directly Grown on Silicon

Prashanth Bhasker, *Member, IEEE*, Justin Norman, John Bowers, *Fellow, IEEE*, and Nadir Dagli, *Fellow, IEEE*

***Abstract*—We report for the first-time electro-optic phase and amplitude modulators in GaAs/AlGaAs epitaxial layers grown on misaligned silicon substrates containing germanium buffer layers. Epilayer has a *npin* doping profile and is equivalent to a *pin* diode. The 4-mm long electrode Mach–Zehnder modulators have 7.4- and 3.6-V V_π under single-arm and push–pull drive conditions corresponding to 1.5 ± 0.1 V-cm modulation efficiency. Data on 7-mm long electrode Fabry–Perot phase modulators indicate 2.3-V Mach–Zehnder modulators are possible. These data also indicate less than 1-dB/cm on-chip propagation loss under 5-V reverse bias.**

***Index Terms*—Compound semiconductors, optical modulation, optical waveguides, phase modulation.**

I. Introduction

OVER the years, developments in CMOS made silicon (Si) as the material of choice for a wealth of applications. The application space covers photonics as well and offers the potential of integration with electronics. The transparency of Si at 1.55 μm and its mature processing technology on silicon on insulator (SOI) platform have resulted in low loss passive waveguides [1]. High index contrast in this material platform enables tightly confined optical mode and compact photonic design. Possibility of compact photonic devices on very large silicon substrates offer significant cost reduction in large volume applications and is one of the most significant drivers for silicon photonics. Even though Si has many advantages in highly integrated passive photonic circuits, its indirect band gap and inversion symmetry limits its use in active components. Due to its indirect bandgap, lasers or optical amplifiers are not possible in Si. Si does not exhibit Pockel's effect due to its inversion symmetry either. This rules-out efficient electro-optic modulator. It is still possible to make modulators using free carrier effects. However, the modulator performance suffers in terms of optical and/or electrical bandwidth, drive voltage and insertion loss. On the other hand, III-V compound semiconductors such as Indium Phosphide (InP), Gallium Arsenide (GaAs) and their alloys such as AlGaAs and InGaAsP are suitable for most of the active component applications lacking in Si. Their direct band gap enables fabrication of lasers and optical amplifiers at telecommunication wavelengths such as 1.3 μm and 1.55 μm. Lack of inversion symmetry in these compound semiconductors allow electro-optic modulators with significantly better performance [2]–[4]. However, these materials are typically grown on InP and GaAs substrates, which are smaller than Si substrates. This is not only a problem for large-scale production, but it also does not allow CMOS electronic integration with superior photonic components. To utilize the bigger silicon substrates that may contain CMOS electronics, significant research efforts have been carried over the past 10 years to integrate III-V epitaxial layers on to a SOI wafer. One such approach involves oxide bonding III-V wafer to Si wafer [5]. Once the III-V growth substrate is removed by wet etching, processing of III-V epi layer begins. Success of this approach greatly depends on the bonding quality, which makes it challenging for mass production. Further, the size and the cost of III-V substrate limits scaling this approach to much bigger silicon wafers. Direct III-V epitaxial growth on Si substrates have been gaining attention over the recent years. Lattice constant and thermal expansion coefficient mismatch between III-V layers and Si results in dislocations during the epitaxial growth. With certain buffer layers introduced between III-V layers and Si, dislocation density has been brought down to acceptable level. Recently, high performance CW quantum dot lasers operating at 1.3 μm epitaxially grown on miscut Si substrates have been demonstrated using germanium as the buffer layer [6]. In addition, high performance photo-detectors have also been demonstrated in III-V epitaxial layers directly grown on Si substrates [7]. In this letter, we take advantage of this technology and for the first time demonstrate epitaxial GaAs/AlGaAs phase and intensity modulators at 1.55 μm grown on Silicon substrates. Preliminary results of this work were reported in [8]. In this paper, we present further data on IV and CV characteristics, details of fabrication as well as a detailed discussion of the data.

Manuscript received April 4, 2018; revised July 9, 2018; accepted July 25, 2018. Date of publication August 3, 2018; date of current version August 16, 2018. This work was supported in part by the Air Force Research Laboratory under FA8650-15-2-5220 and in part by an NSF Grant 1711446. *(Corresponding author: Nadir Dagli.)*

P. Bhasker and N. Dagli are with the Electrical and Computer Engineering Department, University of California Santa Barbara, Santa Barbara, CA 93016 USA (e-mail: prashanth@umail.ucsb.edu; dagli@ucsb.edu).

J. Norman is with the Materials Department, University of California Santa Barbara, Santa Barbara, CA 93016 USA (e-mail: jnorman@ucsb.edu).

J. Bowers is with the Materials and Electrical and Computer Engineering Departments, University of California Santa Barbara, Santa Barbara, CA 93016 USA (e-mail: bowers@ece.ucsb.edu).

Color versions of one or more of the figures in this paper are available online at http://ieeexplore.ieee.org.

Digital Object Identifier 10.1109/JLT.2018.2863208

II. Device Description

Fig. 1 shows the epitaxial layers used in device fabrication. The epitaxial layers were grown on (100) Si intentionally tilted

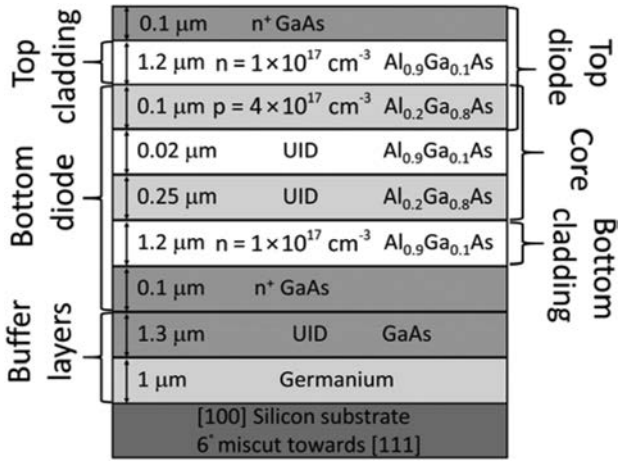

Fig. 1. Epitaxial layers used in device fabrication.

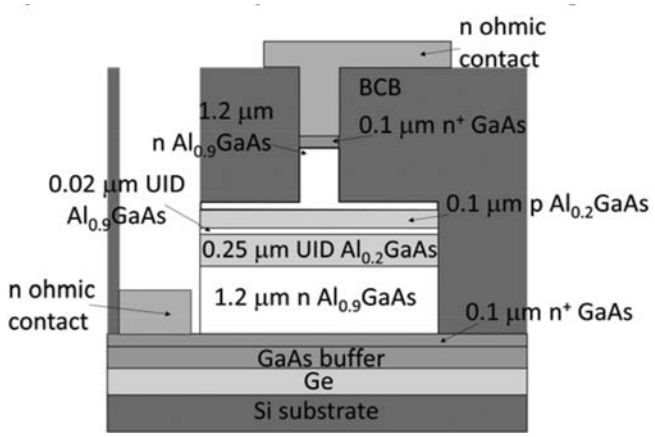

Fig. 2. Cross sectional profile of the optical waveguide, which is also a phase modulator.

6° towards (111). The use of miscut Si substrates was to reduce antiphase domains [9]. Initially buffer layers consisting of 1.3 μm unintentionally doped GaAs on 1 μm unintentionally doped Ge were grown via chemical vapor deposition (CVD) on Si. The as-grown CVD buffer was found to contain a dislocation density of $\sim 2 \times 10^8$ cm^{-2}.

The remaining structure was grown by molecular beam epitaxy (MBE) at 600 °C. Before growing the device layers, two sets of alternating layers of GaAs/AlAs, each 0.2 μm were grown. These layers are not shown in Fig. 1 and do not contribute to device operation. However, they can be used as etch stop layers if the substrate is desired to be removed and epitaxial layers are transferred onto another substrate.

Remaining epitaxial layers contain a slab waveguide in between two heavily doped ($\sim 6.6 \times 10^{18}$ cm^{-3}) n^+ GaAs contact layers. Top and bottom claddings for the slab waveguide is designed to be 1.2 μm thick n doped (1×10^{17} cm^{-3}) $Al_{0.9}Ga_{0.1}As$. These claddings also serve as part of electrodes. Core is designed as unintentionally doped (UID) $Al_{0.2}Ga_{0.8}As$. In GaAs/AlGaAs material system increasing Al concentration reduces the refractive index. The choice of $Al_{0.9}Ga_{0.1}As$ claddings and $Al_{0.2}Ga_{0.8}As$ core provides a large index step, which improves the vertical confinement of the optical mode. Increasing the Al concentration difference between the core and claddings can further increase the confinement but AlGaAs layers with more than 90% Al are susceptible to rapid oxidation in air during processing. $Al_{0.2}Ga_{0.8}As$ has bandgap greater than twice the value of photon energy at 1.55 μm hence two-photon absorption is reduced significantly. This improves the optical power handling of the device. Core also contains a 0.1 μm p $Al_{0.2}Ga_{0.8}As$ with a doping concentration of 4×10^{17} cm^{-3}. A 0.02 μm UID $Al_{0.9}Ga_{0.1}As$ serves as a barrier between the p and UID doped $Al_{0.2}Ga_{0.8}As$ layers. In this design, optical mode is entirely contained within the core and claddings and there is no mode interaction with heavily doped GaAs layers as well as the buffer layers and Si substrate.

Electrically the optical waveguide doping profile is *npin* [10] which is equivalent to back to back diodes connected in series. Top diode consists of n^+ GaAs/n $Al_{0.9}Ga_{0.1}As$/p $Al_{0.2}Ga_{0.8}As$. The bottom diode is a *pin* diode out of p $Al_{0.2}Ga_{0.8}As$/UID $Al_{0.9}Ga_{0.1}As$/UID $Al_{0.2}Ga_{0.8}As$/n $Al_{0.9}Ga_{0.1}As$. Depending on bias polarity, one of the diodes will be forward biased and the other one will be reverse biased. Since diodes are connected in series, only the very small reverse leakage current of the reverse biased diode will flow through forward biased diode. This results in very low voltage drop across the forward biased diode and almost of all the applied voltage drops across reverse biased diode. For AC operation, the diodes can be modeled as two capacitors connected in series. Under device operation, top *pn* diode is forward biased and bottom *pin* diode is reverse biased. The capacitance of the forward biased top diode is much greater than the bottom *pin* diode because of the thick *i*-region in the bottom reverse biased *pin* diode. Since these capacitors are connected in series, effective capacitance is equivalent to that of *pin* diode. Hence, *npin* design effectively works as a *pin* design with the added advantage of having low resistance *n* ohmic contacts. Choosing the bias polarity such that bottom *pin* diode is reverse biased allows the application of large electric fields overlapping very well with the optical mode. This results in efficient modulation. One concern is the presence of *p* doing within the core of the waveguide and the associated free carrier absorption loss. This is dealt with by keeping a high bias across the device so that most of the *p* layer is depleted and the overlap of this later with the optical mode is reduced significantly. Additional free carrier absorption loss originating from n $Al_{0.9}Ga_{0.1}As$ layers is minimal due to low carrier concentration. n^+ GaAs layers do not overlap with the mode and do not contribute any optical loss.

Drive voltage of an electro-optic modulator is directly proportional to thickness of *i*-region with high electric field. It is also inversely proportional to the overlap of optical mode with *i*-region respectively. So passive waveguide was designed to be a rib waveguide to maximize this overlap while simultaneously maintaining the single mode condition required for modulator operation. This waveguide is shown in Fig. 2 and is 1.8 μm wide and is etched 1.2 μm deep. 1.2 μm deep etch includes 0.1 μm n^+ GaAs and 1.1 μm n $Al_{0.9}Ga_{0.1}As$. n $Al_{0.9}Ga_{0.1}As$ was not completely etched to maintain single mode condition. Optical field intensity is designed to be maximum in the UID $Al_{0.2}Ga_{0.8}As$.

Overlap of the optical mode with the UID $Al_{0.2}Ga_{0.8}As$ core, top and bottom *n* $Al_{0.9}Ga_{0.1}As$ are 52.5%, 11.7% and 17.5% respectively. Overlap with undepleted *p* region is 14.4%.

Fabricated phase modulators are the same as the straight waveguide. Mach Zehnder Intensity modulators are also fabricated using two such phase modulators in arms of a regular Mach Zehnder interferometer formed with two y-branches made out of the same waveguide.

III. Device Fabrication

Details of the processing steps are schematically illustrated in Fig. 3. Processing started by lifting off Ni/Ge/Au/Ni/Au 5/18/132/20/1200 nm contact metal on highly doped n^+ GaAs. Next 500 nm thick PECVD oxide was deposited and used as an oxide hard mask for waveguide etching. Oxide was patterned using CHF_3 plasma in an ICP etcher and a photo resist hard mask. After stripping off the photoresist, 1.8 μm wide rib waveguide etch was performed using Cl_2/N_2 plasma. This was followed by a 20 μm wide mesa dry etch that stops on bottom *n* $Al_{0.9}Ga_{0.1}As$. Remaining *n* $Al_{0.9}Ga_{0.1}As$ was wet etched using buffered hydrofluoric acid. Effective mesa width reduced to 16 μm due to undercutting of $Al_{0.9}Ga_{0.1}As$ during wet etching. The same *n* contact metal used before was lifted off on the bottom n^+ GaAs. At this point the sample was annealed at 430 °C for 30 seconds in forming gas to make the top and bottom contacts ohmic. Sample was then subjected to selective (50 μm by 50 μm) proton implantation on *y*-branches to electrically isolate the arms of the interferometer. Three different proton implants with different energies and doses were used to make n^+ GaAs, *n* $Al_{0.9}Ga_{0.1}As$ and *p* $Al_{0.2}Ga_{0.8}As$ layers highly resistive to create electrical isolation between the arms. Sample was then planarized with 4.4 μm thick BCB. BCB was blanket etched without any patterning in CF_4 plasma until the top contacts were fully or nearly exposed. At this point 50/500 nm Ni/Au metal pads were lifted off to have electrical access to top contacts. Finally, BCB was etched to reach the bottom metal contacts. At this stage sample was thinned down to 200 μm thickness using lapping. This was followed by cleaving to form facets. SEM picture of a cleaved facet is shown in Fig. 4.

Even though substrate was misaligned, it was possible to get good facets if substrate was sufficiently thinned down.

IV. Experimental Results

After device fabrication and facet formation, electrical and optical measurements were performed. Even though a proton implantation was used to isolate arms, this implant does not go deep enough to reach the bottom n^+ GaAs contact layer. Implantation only isolates top *n* and *p* layers on both arms. Furthermore, since mesa etch stops on n^+ GaAs contact layer this highly conducting layer extends under all devices. It could be possible to provide device-to-device isolation using a second etch to remove this layer in between individual devices. However, without this etch, it is still possible to make measurements if this layer is kept as an electrical ground. The resistance between two arms as measured between the top *n* ohmic contacts is more than 8 MΩ, which is sufficient to prevent any significant current running between both the arms during device operation.

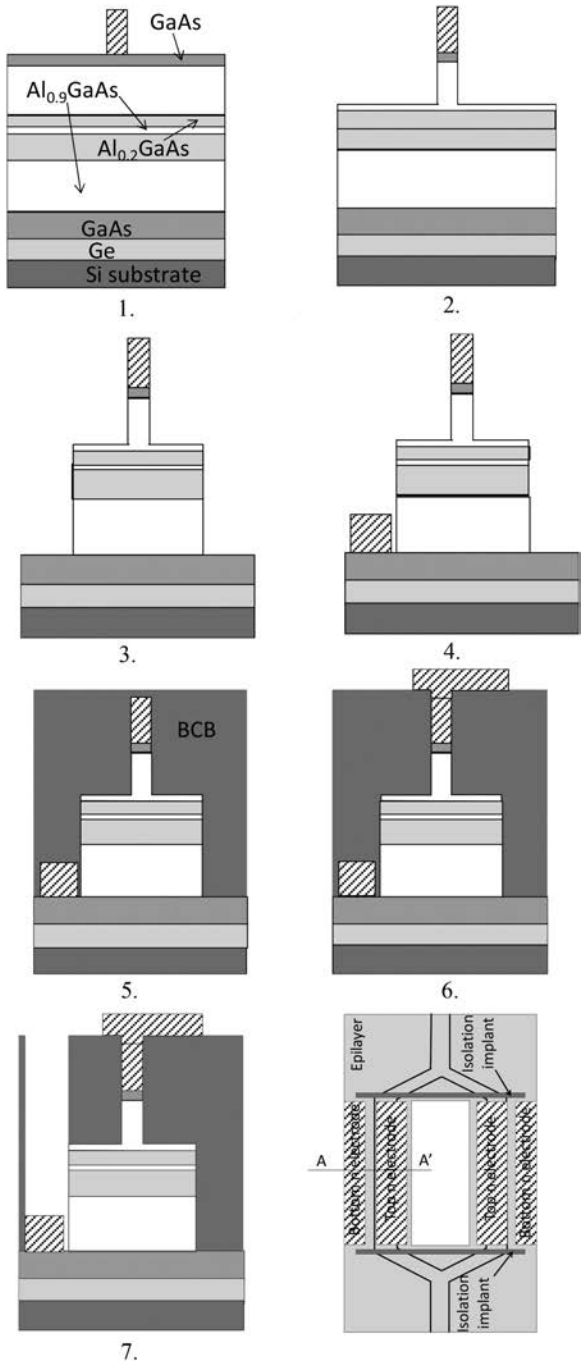

Fig. 3. Process steps used in device fabrication and top schematic of a finished Mach-Zehnder modulator. Cross sectional profile shown in 7 is at AA'. 1. Top n^+ GaAs contact metal. 2. Waveguide etching. 3. Mesa etching. 4. Bottom n^+ GaAs contact metal. 5. Annealing and BCB planarization. 6. Top contact metal pad. 7. Bottom contact opening.

Grounding the bottom n^+ GaAs layer and applying a positive voltage to top n^+ GaAs reverse biases the top diode and a negative voltage reverse biases the bottom *pin* diode. Current voltage (IV) characteristics of a 5 mm long electrode arm is shown in Fig. 5. Along the positive sweep, which reverse biases the top diode, device breaks down at 5 V. On the negative sweep, when the lower *pin* diode is reverse biased device breaks down at -11 V. Doped layers deplete under reverse bias and break down occurs when *p* $Al_{0.2}Ga_{0.8}As$ depletes completely.

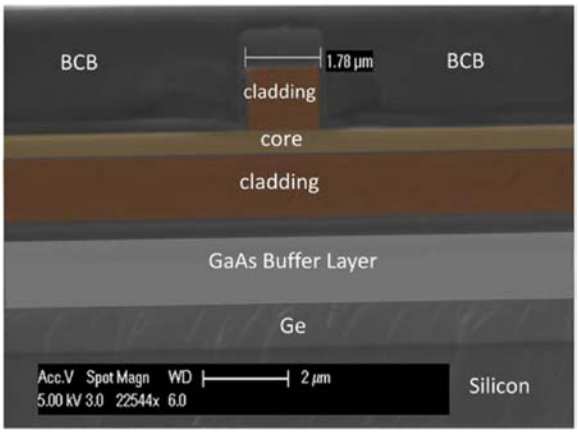

Fig. 4. SEM picture of a cleaved facet. The layers between the lower cladding and GaAs buffer layer are etch stop layers, which do not contribute to device operation.

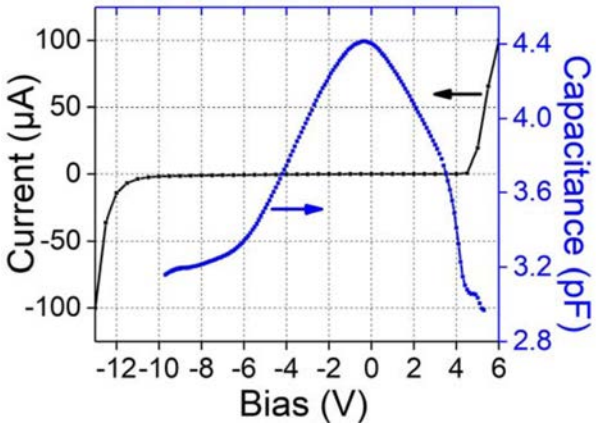

Fig. 5. Current voltage and capacitance voltage characteristics of a 5 mm long Mach-Zehnder modulator arm.

Then current starts to flow between two *n* doped layers. Current is less than 0.1 μA until the break down point for each polarity, which indicates good material quality. Since the lower diode is a *pin* diode it takes a higher voltage to reach the electric field needed to deplete the *p* layer.

Fig. 5 also shows the capacitance voltage (CV) characteristics of the same device. Capacitance decreases rapidly for both diodes as reverse bias increases. This indicates depletion of *p* and *n* layers as well as the sweep out of charge due to unintentional dopants in the *i* layer of *pin* diode. Capacitance of the *pin* diode starts to flatten out after 6 V reverse bias. This indicates full depletion of the *i* layer and any further reduction is due to depletion of *p* and *n* layers. Furthermore, there is depletion of the *p* layer in the core, which helps to reduce the free carrier absorption. At this point a large electric field is generated in the *i* layer, which is most of the core of the optical waveguide. This field overlaps very well with the optical mode and the most efficient modulation results. For lower bias high capacitance indicates that electric field exists only in part of the *i*-region. Hence, overlap of the field with the optical mode is reduced. For these reasons during operation, arms are biased at a bias point corresponding to a high reverse bias of the *pin* diode. Then a modulation voltage is superimposed on the bias voltage.

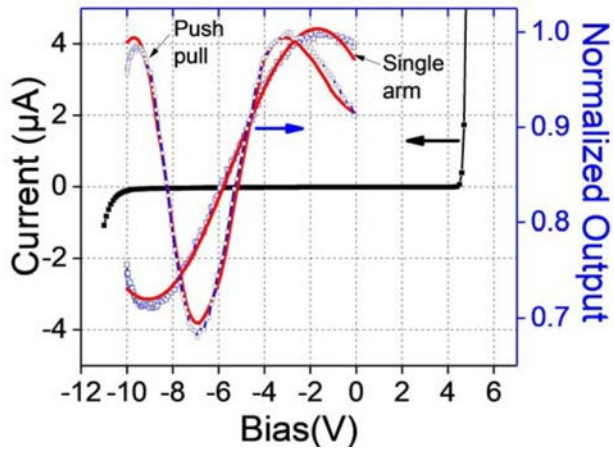

Fig. 6. IV characteristics and optical transfer function of an MZM for 4 mm long electrodes at 1.55 μm.

This way a single arm operation or push pull operation of the modulator is possible. For push pull operation bias is kept the same on both arms but the polarity of the modulating voltage is reversed between the arms.

IV characteristics and optical transfer function of an intensity modulator with 4 mm long electrodes is shown in Fig. 6. IV behavior is very similar to the data presented in Fig. 5. In the optical transfer function dots are the data points and the continuous curve is a curve fit. Based on this curve fitting, when the device is biased at -5 V, the drive voltage under single arm and push pull operation is 7.4 V and 3.6 V respectively.

This corresponds to a drive voltage-length product ($V_\pi L$) of 1.5 ± 0.1 V-cm. V_π shows bias dependence. It is observed that modulation becomes more efficient as reverse bias increases as evidenced by decreased V_π in the higher reverse bias region. This is due to sweep out of the unintentional charge in the *i* layer. Under lower reverse bias V_π is higher. This is related to unintentional doping as evidenced in the CV data under lower reverse biases. At lower reverse biases, this charge screens the electric field as well as reducing the overlap of the field with the optical mode. These two effects increase V_π. Very negligible current indicates no index change due to device heating or carrier injection.

Accurate calculation of V_π requires precise details of the device. In this case, layer thicknesses and doping of the doped layers are well known. However, residual doping in the unintentionally doped *i*-layers is not known. CV data in Fig. 5 shows that there is some level of doping in the 0.25 μm thick $Al_{0.2}Ga_{0.8}As$ *i*-layer. This depletes under high reverse bias but there is not full depletion in the bias range where transfer functions shown in Fig. 6 are measured. Although this doping level is low and is not expected to change the V_π significantly compared to fully depleted case, it is hard to estimate the exact thickness of the high electric field region and the mode overlap with this field. However, there is almost full depletion in the bias range from -8 V to -10 V and V_π due to electro-optic effect can be estimated using the well-known expression under push pull operation, which is $V_\pi = \lambda g / 2L\Gamma n_e^3 r_{41}$. We find the thickness of the high field region around 9 V reverse bias as $g = 0.4$ μm based on numerical simulations. Then using calculated values $n_e = 3.1$, $\Gamma = 0.57$

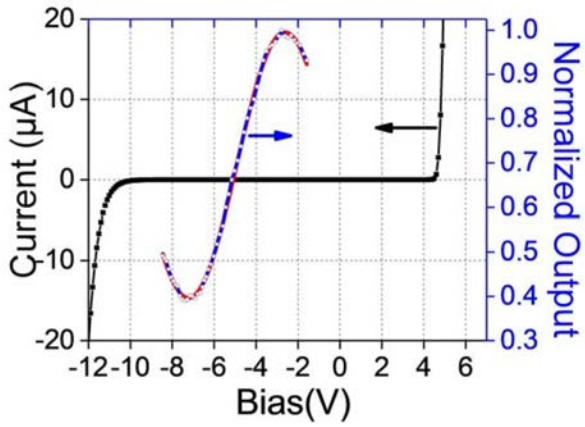

Fig. 7. IV characteristics and normalized optical transmission of a 7 mm long Fabry-Perot modulator with 7 mm long electrodes at 1.55 μm.

along with $r_{41} = 1.2 \times 10^{-12}$ m/V and $L = 1$ cm we estimate V_π as 1.52 V-cm. This is very close to the measured value. This calculation takes into account only the index change due to linear electro-optic effect. In addition, there could be further index change due to carrier depletion in the doped regions. However, the extend of the depletion in the doped layers is very low. In this case major free effect contribution will be due to heavily doped *p* $Al_{0.2}Ga_{0.8}As$ layer depletion. Based on numerical calculations, around 9 V reverse bias this layer depletes only 0.04 μm. As a result, overlap of the optical mode with the doped layers is very low. We estimate the carrier depletion induced refractive index change to be less than 10%.

Extinction ratio is limited mainly by the mesa modes, which are excited at the input. Light in the mesa modes are even present during the off state of the modulator leading to low extinction ratio.

Fig. 7 shows the normalized transmission of a Fabry-Perot modulator along with the IV characteristics. Fabry-Perot modulator is formed between the input and output facets of a straight waveguide. In this case, both the length of the modulator and the electrode are 7 mm. Points show the data taken at 1.55 μm and continuous curve is the fit. Under 5 V reverse bias V_π is 4.6 V. A push pull driven MZM using this phase modulator in the arms would have a V_π of 2.3 V. This data also indicates on chip propagation loss of less than 1 dB/cm using a facet reflectivity of 0.26 calculated using the plane wave reflection coefficient with $n_e = 3.1$. This is actually an estimate due to presence of mesa modes, which affect the fringe contrast, but shows a very favorable propagation loss.

Devices reported here are fairly long and high speed operation can be achieved using a traveling wave design. In our previous work, we demonstrated modulators with bandwidth exceeding 40 GHz in similar structures using a loaded line traveling wave electrodes [4]. Therefore, with appropriate design similar bandwidths can be obtained for these devices.

V. Conclusion

This paper reports for the first-time electro-optic phase and amplitude modulators in GaAs/AlGaAs epitaxial layers grown on Si substrates. Substrate used is (100) Si intentionally tilted 6° towards (111). It also has a 1 μm thick Ge buffer layer to reduce the dislocation density of the GaAs/AlGaAs epitaxial layers grown by MBE. Epilayer has *npin* doping profile and is shown to be equivalent to a *pin* design under appropriate bias. The IV characteristics indicate less than 0.1 μA current under operating conditions. CV data shows the presence of unintentional doping in the *i*-region. This charge is swept out after about 6 V reverse bias and efficient modulation results. However presence of this charge makes V_π bias dependent. V_π is higher at lower reverse bias due to screening out of electric field and reduced overlap factor. Results indicate 4 mm long electrode Mach-Zehnder modulators with 7.4 and 3.6 V V_π under single arm and push pull drive conditions. This corresponds to 1.5 ± 0.1 V-cm modulation efficiency. Data on 7 mm long electrode Fabry-Perot phase modulators indicate 2.3 V Mach-Zehnder modulators are possible. This data also indicates less than 1 dB/cm on chip propagation loss under 5 V reverse bias. These results are comparable to the best-reported results in bulk GaAs/AlGaAs modulators [11]. These results combined with the potential of integration with lasers, detectors and other passive components on epilayers grown on large Si substrates open up large-scale high performance III-V photonic integration.

Acknowledgment

The authors would like to thank A. Gungor for helping in substrate thinning.

References

[1] J. F. Bauters *et al.*, "Silicon on ultra-low-loss waveguide photonic integration platform," *Opt. Exp.*, vol. 21, no. 1, pp. 544–555, 2013.
[2] J. H. Shin and N. Dagli, "Ultra-low drive voltage substrate removed GaAs/AlGaAs electro-optic modulators at 1550 nm," *IEEE J. Sel. Topics Quantum Electron.*, vol. 19, no. 6, Nov./Dec. 2013, Art. no. 3400408.
[3] S. Dogru and N. Dagli, "0.2 V drive voltage substrate removed electro-optic Mach-Zehnder modulators with MQW cores at 1.55 μm," *IEEE/OSA J. Lightw. Technol.*, vol. LT-32, no. 3, pp. 435–439, Feb. 1, 2014.
[4] S. Dogru and N. Dagli, "0.77-V drive voltage electro-optic modulator with bandwidth exceeding 67 GHz," *Opt. Lett.*, vol. 39, no. 20, pp. 6074–6077, Oct. 15, 2014.
[5] A. W. Fang *et al.*, "Electrically pumped hybrid AlGaInAs-silicon evanescent laser," *Opt. Exp.*, vol. 14, no. 20, pp. 9203–9210, 2006.
[6] A. Y. Liu *et al.*, "High performance continuous wave 1.3 μm quantum dot lasers on silicon," *Appl. Phys. Lett.*, vol. 104, no. 4, 2014, Art. no. 041104.
[7] Y. Gao et al., "High-Speed normal-incidence p-i-n InGaAs Photodetectors grown on silicon substrates by MOCVD," *IEEE Photon. Technol. Lett.*, vol. 24, no. 4, pp. 237–239, Feb. 2012.
[8] P. Bhasker, J. Norman, J. Bowers, and N. Dagli, "Intensity and phase modulators in epitaxial III-V layers directly grown on silicon operating at 1.55 μm," in *Proc. Frontiers in Optics*, Washington, DC, USA, 2017, Paper FTh4A.3.
[9] K. Adomi *et al.*, "Characterization of GaAs grown on Si epitaxial layers on GaAs substrates," *J. Appl. Phys.*, vol. 69, no. 1, pp. 220–225, 1991.
[10] S. Dogru, J. H. Shin, and N. Dagli, "InGaAlAs/InAlAs multi quantum well substrate removed electro-optic modulators," in *Proc. IEEE Photonic Society Annual Meeting*, Arlington, VA, USA, Oct. 9–13, 2011, pp. 739–740, Paper ThJ2.
[11] J. H. Shin, S. Wu, and N. Dagli, "35 GHz bandwidth, 5 V-cm drive voltage, bulk GaAs substrate removed electro optic modulators," *IEEE Photon. Technol. Lett.*, vol. 19, no. 18, pp. 1362–1364, Sep. 15, 2007.

Prashanth Bhasker (M'18) received the B.E. degree from Anna University, Chennai, India. He is currently working toward the Ph.D. degree with the Electrical and Computer Engineering Department, University of California at Santa Barbara, CA, USA. His interests are design, fabrication, and testing of advanced photonic components.

Justin Norman received the B.S. degrees in physics and chemical engineering from the University of Arkansas, Fayetteville, AR, USA, in 2013. He is currently working toward the Ph.D. degree with the Materials Department, University of California, Santa Barbara, CA, USA, as an NSF and Frenkel Foundation Fellow. His research interests include molecular beam epitaxial growth of InAs quantum dot lasers on silicon, direct III–V growth on Si, and quantum dot microcavities for cavity quantum electrodynamics.

John Bowers (F'94) received the M.S. and Ph.D. degrees from Stanford University, Stanford, CA, USA. He is the Director with the Institute for Energy Efficiency and a Distinguished Professor with the Departments of Electrical and Computer Engineering and Materials, University of California, Santa Barbara (UCSB), CA, USA. He worked for AT&T Bell Laboratories and Honeywell before joining UCSB. His research interests are primarily concerned with silicon photonics, optoelectronic devices, optical switching, and transparent optical networks and quantum dot lasers. He is a Fellow of the OSA and the American Physical Society, and was the recipient of the IEEE Photonics Award, OSA/IEEE Tyndall Award, the IEEE LEOS William Streifer Award, and the South Coast Business and Technology Entrepreneur of the Year Award. He is a member of the National Academy of Engineering and the National Academy of Inventors.

Nadir Dagli (F'06) received the Ph.D. degree in electrical engineering from the Massachusetts Institute of Technology, Cambridge, MA, USA, in 1986. After graduation, he joined the Electrical and Computer Engineering Department, University of California at Santa Barbara, CA, USA, where he is currently a Professor and the Chairman. His current research interests are design, fabrication, and modeling of guided-wave components for optical integrated circuits, ultrafast electro-optic modulators, WDM components and photonic nanostructures. He served and chaired many technical program and other professional committees. He was the Editor-in-Chief of the IEEE PHOTONICS TECHNOLOGY LETTERS 2000–2005 and an elected member of the IEEE-LEOS board of governors 2003–2005.